

Nanoscale capillary wetting studied with dissipative particle dynamics

Claudio Cupelli,^{1,*} Björn Henrich,^{2,*} Michael Moseler,^{2,3} and Mark Santer^{1,†}

¹ *Laboratory for MEMS applications (Chair Prof. R. Zengerle),
Department of Microsystems Engineering(IMTEK), University of Freiburg,
Georges-Koehler-Allee 106, 79110 Freiburg, Germany*

² *FMF-Freiburger Materialforschungszentrum, University of Freiburg,
Stefan Meier Str. 21, 79104 Freiburg, Germany*

³ *Fraunhofer Institute for Mechanics of Materials, Wöhlerstr. 11, 79108 Freiburg, Germany*
(Dated: September 14, 2018)

We demonstrate that Multi-Body Dissipative Particle Dynamics (MDPD) can be used as an efficient computational tool for the investigation of nanoscale capillary impregnation of confined geometries. As an essential prerequisite, a novel model for a solid-liquid interface in the framework of MDPD is introduced, with tunable wetting behaviour and thermal roughening to reduce artificial density- and temperature oscillations. Within this model, the impregnation dynamics of a water-like fluid into a nanoscale slit pore has been studied. Despite the coarse graining implied with the model fluid, a sufficient amount of non-equilibrium averaging can be achieved allowing for the extraction of useful information even from transient simulations, such as the dynamic apparent contact angle. Although it is found to determine the capillary driving completely, it cannot be interpreted as a simple function of the capillary number.

PACS numbers: 47.61.-k, 47.60.+i, 47.11.-j, 68.08.-p, 68.03.-g

Introduction. Over the last decade, continuous, meso-scale particle simulation methods such as Dissipative Particle Dynamics (DPD)[1, 2] and many variants thereof [3, 4, 5] have received considerable attention. Originally invented to include hydrodynamic effects in meso scale simulations of simple and complex fluids [1, 6], it also has successfully been employed for studying polymeric systems or melts [7, 8, 9] or lipid membranes [10], and for colloidal suspensions [11, 12]. As a model for solvents, one of the most important recent developments is the introduction of cohesive properties [13, 14, 15], extending the simple quadratic dependance on density in the equation of state (EOS) in early formulations [2]. The approach of Warren [15] leads to particularly stable liquid-vapor interfaces and could be of great value in studying free-surface fluid dynamics problems where thermal capillary fluctuations are important, such as the intriguing phenomena related to the nanoscale Rayleigh instability (e.g. the break-up of liquid nano jets [16]). In most numerical studies involving fluid particle (FP) [17] methods, the investigations have largely been kept generic. Specific interactions, e.g., between solid-liquid interfaces, have only been accounted for in crude ways, since in the majority of cases, the FP-interactions do not arise from a systematic coarse graining procedure starting at the atomistic scale. We nevertheless suggest that a FP method can still be suitable for studying the aforementioned phenomena, provided that adhesive and interfacial properties are introduced carefully and with respect to the

intrinsic molecular characteristics of a given FP model. It is the purpose of this paper to outline how this could be achieved, and we demonstrate for the capillary filling of a narrow slit pore that detailed information from short term transient simulations can be extracted.

General Theory. Although the simulation scheme for FP-methods is MD-like in character, it employs two features notably different from traditional MD-simulations: soft interaction potentials of a finite range r_c , and a momentum conserving thermostat contributing a major part to the viscosity of the liquid [4, 18]. In DPD, particles interact via pairwise central forces $\mathbf{F}_{ij} = \mathbf{F}_{ij}^R + \mathbf{F}_{ij}^D + \mathbf{F}_{ij}^C$. If \mathbf{r}_i denotes the particle position, the conservative force in standard DPD is $\mathbf{F}_{ij}^C = Aw^C(r_{ij})\mathbf{e}_{ij}$, where $\mathbf{r}_{ij} = \mathbf{r}_i - \mathbf{r}_j$, $r_{ij} = |\mathbf{r}_{ij}|$ and $\mathbf{e}_{ij} = \mathbf{r}_{ij}/r_{ij}$. The weight function $w^C(r) = (1 - r/r_c)$ vanishes for an inter-particle distance r larger than a cutoff radius r_c . The random and dissipative forces are $\mathbf{F}_{ij}^R = qw^R(r_{ij})\xi_{ij}\mathbf{r}_{ij}$ and $\mathbf{F}_{ij}^D = -\gamma w^D(r_{ij})(\mathbf{v}_{ij} \cdot \mathbf{e}_{ij})\mathbf{e}_{ij}$, respectively, and act as a thermostat if the amplitudes q of the random variable ξ_{ij} and the viscous dissipation γ satisfy a fluctuation-dissipation theorem: $q^2 = 2\gamma k_B T$ and $w_{ij}^R(r)^2 = w_{ij}^D(r)$. The usual choice for the weight functions is $w^R = w^C$. Then, the EOS becomes at most quadratic in the FP-density ρ , excluding the existence of capillary surfaces. However, \mathbf{F}_{ij}^C may be augmented by density dependent contributions [13, 14, 15] in order to achieve arbitrary EOS. This class of schemes is termed multi-body DPD (MDPD). Here, the approach of Warren [15] is pursued who has the repulsive part of the force depend on a weighted average of the particle density, while the attractive part is density independent:

$$\mathbf{F}_{ij}^C = A_{ij}w^C(r_{ij})\mathbf{e}_{ij} + B(\bar{\rho}_i + \bar{\rho}_j)w_d(r_{ij})\mathbf{e}_{ij}, \quad (1)$$

*Both authors contributed equally to this work.

†Electronic address: santer@imtek.de

TABLE I: Parameters used in the simulations. The surface tension has been obtained in a planar geometry, by integrating the lateral part of the pressure tensor in normal direction. The characteristic fluid parameters are given in model units [m.u.] and in real units (MKS), where $N_m \simeq 3$. Note, that the time step Δt for the numerical integration of the MDPD equations is 2 orders of magnitude larger than Δt in a comparable MD simulation.

Parameter	Symbol	m.u.	MKS
Fluid particle density	ρ	6.00	(1000kg/m ³)
Interaction range (attr.)	r_c	1.0	(0.82nm)
Interaction range (rep.)	r_d	0.75	
Amplitude of \mathbf{F}^R	q	6.00	
Compress.	$\partial p / \partial \rho$	45 ± 2	
Surface Tension	σ	7.51 ± 0.04	(0.138N/m)
Viscosity	η	7.41 ± 0.06 ^a	(0.0003Pa s)
MDPD time step	Δt	0.02	76 fs

^aThe viscosity was determined by a fit to a Poiseuille velocity profile for a pressure driven flow in a slit of width b .

with an additional weight function $w^d(r) = (1 - r/r_d)^2$. For a single particle species, $A_{ij} \equiv A$ is negative; the repulsive part with $B > 0$ acts at a slightly *smaller* radius of interaction r_d . $\bar{\rho}_i$ at the location of particle i is the instantaneously weighted average $\bar{\rho}_i = \sum_{i \neq j} w_d(r_{ij})$. Warren showed that this approach produces stable capillary surfaces. In addition, we introduce a species dependent force constant A_{sl} , defining the interaction between liquid(l) particles and those of the solid(s) wall. The parameters we use for this model ($A = -40.0$, $B = 25.0$) vary slightly from the ones in [15]. The length scale in real space is derived by matching the compressibility $\partial p / \partial \rho$ of the real fluid (water) to the one of the model fluid over a particle renormalization factor (the coarse graining level) N_m , as outlined in [10]. Formally, N_m is the number of actual molecules a single fluid particle is to represent. The unit of time is set equal to r_c / v_{th} , where v_{th} means the (real) thermal velocity of one fluid particle with mass N_m times the molar mass of a water molecule. This is independent of the transport properties of the system, as opposed to other prescriptions [2]. All relevant quantities of our MDPD liquid are summarised in Table I. We stress that the case $N_m = 1$ would *not* correspond to an atomistic limit; the MDPD liquid always remains a molecular substitute fluid, the molecular characteristics of which must be compared with the (continuum) phenomena studied. *An adequate wall model.* With FP approaches, there are roughly two classes of strategies to construct solid walls: (i) use of virtual boundary planes [19] and (ii) walls made of frozen or crystalline arrangements of fluid particles [20, 21]. In (i), some rule must be given to reintroduce a particle to the liquid when it crosses the boundary, whereas in (ii) the wall acts directly over interparticle forces. Models for sharp,

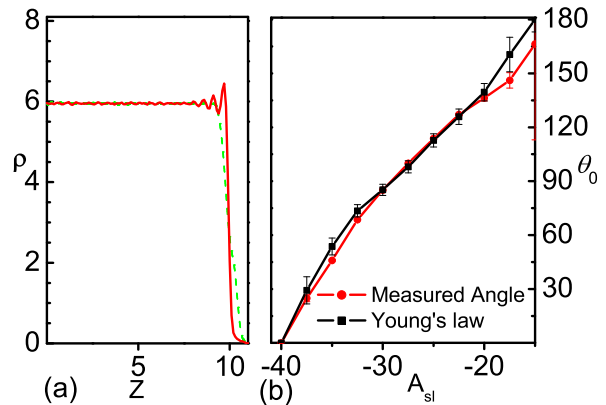


FIG. 1: (color online) (a) Density distribution within a half-slit (full width $20r_c$) for a mutual attraction strength, $A_{sl} = -40.0$ for a rigid wall (red line) and thermally roughened wall (green line). For a rigid wall unphysical density oscillations occur near the wall. (b) Variation of contact angle with varying A_{sl} , as determined from a simulated optical measurement (\bullet), or using Young's law: $\sigma_{sv} = \sigma_{sl} + \sigma_{lv} \cos(\theta_0)$, and obtaining σ_{sl} from integrating the lateral pressure tensor in planar geometry (\blacksquare).

rigid interfaces will usually produce order effects and thus density oscillations that on the targeted length scale are not expected. Also, inhomogeneous temperature profiles may arise [22], or other spurious effects (detachment of droplets under shear flow [21]). In this work, we shall use a thermally roughened wall and allow fluid particles to penetrate the solid-liquid interface slightly. To achieve thermodynamic compatibility, the solid phase is made of fluid particles at the *same* density as the fluid, resulting in a strictly homogeneous temperature profile across the interface. The wall particles are pinned by harmonic forces to their initial position, and mutually interact via ordinary MDPD forces (eq. (1) with $A_{ss} = -40.00$). An additional, soft harmonic force acting normal to the interface prevents single fluid particles from diffusing into the wall indefinitely. Fig. 1 illustrates density profiles and the variation of the static contact angle of this solid-liquid interface. In contrast to a conventional rigid wall density oscillations can be much reduced (compare red and green lines in Fig. 1a, corresponding to two different strengths of the pinning force). Note that the wetting behaviour of the wall can be tuned arbitrarily between hydrophilic and hydrophobic by diminishing the mutual interaction A_{sl} between solid- and liquid particles. The interfacial energy can be measured with respect to a planar interface, by integrating over the transverse part of the pressure tensor; the static contact angle θ_0 resulting from the Young-Laplace equation is in excellent agreement with an optical measurement (cmp. Fig. 1b), where θ_0 is determined from the meniscus shape of a liquid slab

trapped between parallel walls. Details about this model of a solid-liquid interface will be published elsewhere [23].

Dynamic behaviour of the impregnation process. In order to demonstrate the applicability of our interface model to nanoscale impregnation, we study the dynamics of a water-like liquid in a slit pore of width $b = 20 \text{ nm} \simeq 24r_c$ attached to a finite reservoir (see Fig. 2a for technical details). We consider the case where $\theta_0 = 0$, (i.e. $A_{sl} = -40.0$). Fig. 2b and c depict snapshots of the meniscus at two different times during impregnation. Partly due to pronounced capillary oscillations that are excited along with the release in free energy during impregnation, the meniscus deviates from a spherical shape. By ignoring contributions of the wedges, an apparent dynamic contact angle $\theta_d(t)$ can be extracted by a fit to a circle segment (red dashed lines in Fig. 2b,c). The evolution of $\cos(\theta_d(t))$ and the penetrated height $z(t)$ over time (red solid lines in Fig. 2d, e) can be divided into two regimes. While for $t < 0.35 \text{ ns}$ the liquid motion is dominated by inertia and high velocities, resulting in a rapid increase of θ_d , a slow decrease towards the static contact angle can be observed for later times. It is important to note that the spatial dimensions and time scales probed here (the hydrodynamic time scale τ_h and the relevant capillary oscillation period τ_{osc}) are still well above the intrinsic molecular scales of the model fluid [26]. This suggests that phenomenologically, the impregnation dynamics should follow some continuum law (as it should for a fully atomistic description) balancing viscous, capillary and inertial forces with the momentum change $d/dt(m(t)\dot{z}(t) + \alpha m_{res}(t)\dot{z}_{res}(t))$. Here the time dependent velocities ($\dot{z}(t)$, $\dot{z}_{res}(t)$) and accelerated masses ($m(t)$, $m_{res}(t)$) of the liquid in the slit and a fraction α of the liquid in the reservoir have been introduced. For a slit geometry as given in Fig. 2, the evolution of the height of the meniscus is governed by

$$\rho\dot{z}(c_1\dot{z} + \alpha l_0) + \rho c_1 \dot{z}^2 = \frac{2\sigma}{b} \cos(\theta_d) - \frac{12\eta}{b^2} z\dot{z}, \quad (2)$$

with $c_1 = (1 - ab/b_{res})$, where b/b_{res} denotes the ratio of the slit- to the reservoir width in x -direction. The Laplace pressure on the right hand of Eq. 2 side is the driving force of the impregnation and consequently one expects the dynamics solely to be determined by the time dependent behaviour of the (apparent) dynamic contact angle θ_d . This is indeed the case: if the measured course of $\cos(\theta_d(t))$ (red solid line in Fig. 2d) is inserted into Eq. 2, a numerical integration results in the dashed-dotted line in Fig. 2e, and is in excellent agreement with the numerically measured $z(t)$, with fluctuations suppressed by viscosity and inertia. As we may speak of an average θ_d , it would now be appropriate to make contact to standard continuum theories using constitutive laws of the form $\theta_d = \theta_d(\text{Ca})$, where here $\text{Ca} = \eta\dot{z}/\sigma$ denotes the capillary number. The straightforward insertion of empirical laws that have been obtained experimentally for a

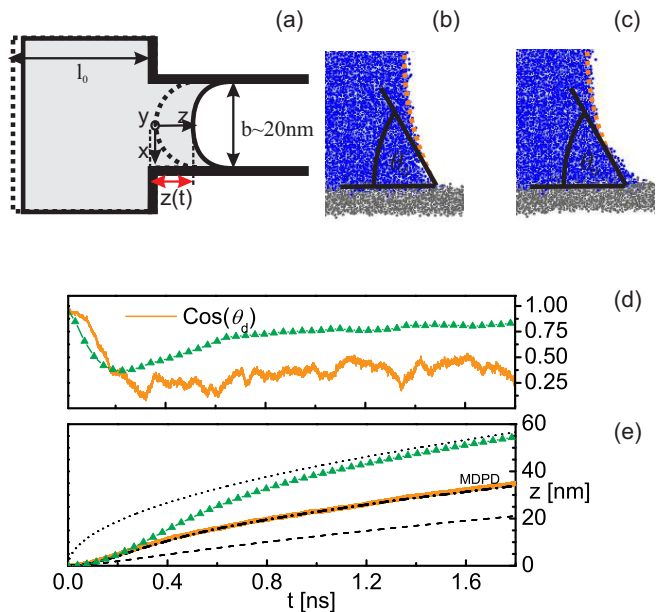


FIG. 2: (color online) Impregnation of a slit pore. While the simulation cell is finite in z -direction, periodic boundary conditions are applied in x and y . The period in y -direction (slit depth) is set to $12r_c$. The simulation involved $\simeq 170,000$ FP, a complete run requiring 36 hrs. on a single processor workstation. (a) Initially, a spherical meniscus with the static contact angle $\theta_0 = 0^\circ$ has been prepared. Panels b and c show snapshots of the dynamic contact angle at later times. Panel d compares the MDPD impregnation dynamics (solid line) with corresponding predictions from various continuum models. The dash-dotted line results from an analogous integration, with the empirical law of Ref. [24]. Triangles (green) represent $\cos(\theta_d)$ (inset) and $z(t)$, with θ_d determined from a stationary MDPD plug flow experiment. Dashed (green): integration of Eq. 2 with driving Laplace-pressure derived from the measured dynamic contact angle θ_d , see inset for $\cos(\theta_d(t))$. As a general reference, the Washburn solution [25], valid for asymptotically large times ($\theta_d \simeq \theta_0$), is displayed.

similar range of Ca as found here ($\text{Ca} \simeq 0 - 0.13$) fails in general (see the law of Joos and Bracke [24] as an example, Fig. 2e, dashed line). Analysing $\theta_d(\text{Ca})$ in terms of theoretical models such as a chemical or a hydrodynamic model [27] or combinations thereof [28], however, is possible but appears not to be very conclusive. Rather, it is instructive to extract a constitutive law $\theta_d(\text{Ca})$ from a steady state MDPD simulation with stationary flow profile. For the relevant range of Ca , a sufficiently long fluid plug is driven at constant speed v through an infinite slit pore with the same width as in the impregnation study. The capillary oscillations are much reduced in this setup, and the meniscus profile and θ_d can be extracted in a co-moving frame. If we then insert the resulting $\theta_d(\text{Ca}(v = \dot{z}(t)))$ into Eq. 2, the deviation from the measured impregnation is *again* significant (green triangles in Fig. 2d,e).

Discussion and conclusions. The apparent “failure” of the consistency check above is rooted in the implicit assumption that in general, the (apparent) dynamic contact angle is a function of Ca and possibly a small set of parameters: local dissipation mechanisms in a liquid wedge close to or at the triple phase contact line are assumed to govern its mobility [27]. However, the realistic numerical setup (afforded by the numerical benefits of the FP method) and the molecular nature of our solid-liquid model system include aspects that go beyond a simple picture: (i) as the simulation is full 3D, the contact line is not only allowed to undulate in x , but also in y -direction. This should affect its average mobility [28]. (ii) More important, our results suggests that θ_d depends on the flow field as a whole, as the Poiseuille profile of the stationary experiment and the approximate plug flow in the inertial phase of the impregnation process must be opposed [33]. A *functional* dependance of θ_d on the flow field is discussed in [29]; a key feature is the dynamics of interface formation, allowing for nonequilibrium values and gradients in surface and interfacial tension.

It must be emphasized that since the model fluid does not employ atomistic interactions (e.g., of the LJ-type), the continuum aspects of the “true” impregnation dynamics are possibly amplified. Nevertheless, we would like to stress the usefulness of the FP approach as an efficient tool for the exploration of relevant processes close to and at the contact line. In combination with subsequent, careful large scale atomistic verification, FP methods can provide important contributions to a unifying picture of the rich physics occurring in dynamic wetting phenomena.

We gratefully acknowledge the support of Deutsche Forschungsgemeinschaft (DFG), SPP 1164, SA 1052/1-1 and Mo 879/4-1.

-
- [1] P. J. Hoogerbrugge and J. M. V. A. Koelman, *Europhys. Lett.* **19**, 155 (1992).
- [2] R. Groot and P. B. Warren, *J. Chem. Phys.* **107**, 4423 (1997).
- [3] P. Espanol, *Phys. Rev. E* **57**, 2930 (1998).
- [4] C. P. Lowe, *Europhys. Lett.* **47**, 145 (1999).
- [5] E. G. Flekkoy, P. V. Coveney, and G. DeFabritiis, *Phys. Rev. E* **62**, 2140 (2000).
- [6] C. P. Lowe and M. W. Dreischor, *Simulating the Dynamics of Mesoscopic Systems* (Springer, 2004), pp. 39 – 68.
- [7] R. D. Groot and T. J. Madden, *J. Chem. Phys.* **108**, 8713 (1998).
- [8] R. D. Groot, T. J. Madden, and D. J. Tildesley, *J. Chem. Phys.* **110**, 9739 (1999).
- [9] R. D. Groot, *Langmuir* **16**, 7493 (2000).
- [10] R. D. Groot and K. L. Rabone, *Biophys. J.* **81**, 725 (2001).
- [11] E. S. Boek, P. V. Coveney, and H. N. W. Lekkerkerker, *J. Phys. Cond. Mat.* **8**, 9509 (1996).
- [12] E. S. Boek, P. V. Coveney, H. N. W. Lekkerkerker, and P. van der Schoot, *Phys. Rev. E* **55**, 3124 (1997).
- [13] I. Pagonabarraga and D. Frenkel, *J. Chem. Phys.* **115**, 5015 (2001).
- [14] S. Y. Trofimov, E. L. F. Nies, and M. A. J. Michels, *J. Chem. Phys.* **117**, 9383 (2002).
- [15] P. B. Warren, *Phys. Rev. E* **68**, art. no. 066702 (2003).
- [16] M. Moseler and U. Landman, *Science* **289**, 1165 (2000).
- [17] This terminology is chosen for general continuum, meso-particle methods employing unspecific, soft interactions. The shorthand DPD shall indicate the special kind of thermostat associated with a given scheme.
- [18] A. J. Masters and P. B. Warren, *Europhys. Lett.* **48**, 1 (1999).
- [19] M. Revenga, I. Z. P. Espanol, and I. Pagonabarraga, *Int. J. Mod. Phys. C* **9**, 1319 (1998).
- [20] A. T. Clark, M. Lal, J. N. Ruddock, and P. B. Warren, *Langmuir* **16**, 6342 (2000).
- [21] J. L. Jones, M. Lal, J. N. Ruddock, and N. A. Spenley, *Faraday Discuss.* **112**, 129 (1999).
- [22] X. J. Fan, N. Phan-Thien, N. T. Young, X. H. Wu, and D. Xu, *Physics of Fluids* **15**, 11 (2003).
- [23] B. Henrich, C. Cupelli, M. Moseler, and M. Santer (2006), in preparation.
- [24] M. Bracke, F. D. Voeght, and P. Joos, *Progr. Coll. Polym. Sci.* **79**, 142 (1989).
- [25] E. W. Washburn, *Phys. Rev.* **17**, 273 (1921).
- [26] The smallest length scale r_0 is related to the length scale where the density correlation function varies significantly, for the MDPD fluid we have $r_0 \sim 0.6r_c$. The shortest time scale is determined by the decay of the velocity autocorrelation function, representative for a time τ_c at which single fluid particle collisions take place, we find $\tau_c = 0.049 \pm 0.003[\text{m.u.}]$. Continuum behaviour in the sense of generalized hydrodynamics can be assumed if, for a characteristic large wave vector k and a high frequency ω , the inequalities $kr_0 \ll 1$ and $\omega\tau_c \ll 1$ hold [30]. As a rough estimate, one may choose $k = 2\pi/b$ and $\omega = 2\pi/\tau_h$. τ_h is the hydrodynamic time scale $\tau_h = \rho b^2/12\eta$ on which one expects the transition from the inertial to the viscous regime [31]. Although the spatial condition $kr_0 \simeq 0.16 \ll 1$ seems fair, the value of $\omega\tau_c \simeq 0.01 \ll 1$ is satisfactory. As long as there is no excessive local shear gradient, one should expect the validity of generalized hydrodynamics, as also conjectured for other, atomistic contact angle studies [32]. τ_{osc} can be estimated from the dispersion relation $\omega^2 = (\sigma/\rho)k^3$ to be $\simeq 11[\text{m.u.}]$ (with $k = 2\pi/(b/2)$ in x -direction)).
- [27] F. Brochard-Wyart and P. G. de Gennes, *Adv. Coll. Int. Sci* **39**, pp. 1 (1992).
- [28] R. Golestanian and E. Raphaël, *Phys. Rev. E* **64**, art. no. 031601 (2001).
- [29] T. D. Blake, M. Bracke, and Y. D. Shikhmurzaev, *Physics of Fluids* **11**, 1995 (1999).
- [30] J. P. Boon and S. Yip, *Molecular Hydrodynamics* (McGraw-Hill, 1980), re-published by Dover Publications (1991).
- [31] D. Quéré, *Europhys. Lett.* **39**, 533 (1997).
- [32] P. A. Thompson and M. O. Robbins, *Phys. Rev. Lett.* **63**, 766 (1989).
- [33] A difference in flow field has also been noticed in LJ-simulations of sheared liquid slabs, with varying θ_0 ; see Gentner, Ogonowski and De Coninck, *Langmuir* **2003**, 19, pp. 3996.